



Deposition of c-axis orientation aluminum nitride films on flexible polymer substrates by reactive direct-current magnetron sputtering

H. Jin ^{a,*}, J. Zhou ^a, S.R. Dong ^a, B. Feng ^a, J.K. Luo ^{a,b}, D.M. Wang ^a, W.I. Milne ^{c,d}, C.Y. Yang ^e

^a Dept. Info. Sci. & Electron. Eng., Zhejiang University, Hangzhou 310027, China

^b Inst. Mater. Res. & Innovat., Bolton University, Deane Road, Bolton BL3 5AB, UK

^c Electr. Eng. Dept., Cambridge University, Cambridge CB3 0FA, UK

^d Dept. Info. Sci. of Display, Kyung Hee University, Seoul 130701, Republic of Korea

^e Center for Nanostructures, Santa Clara University, Santa Clara, CA 95053, USA

ARTICLE INFO

Article history:

Received 21 July 2011

Received in revised form 7 March 2012

Accepted 7 March 2012

Available online 14 March 2012

Keywords:

Reactive magnetron sputtering

c-Axis orientation

Aluminum nitride

Thin films

Polymer substrates

ABSTRACT

Aluminum nitride (AlN) piezoelectric thin films with c-axis crystal orientation on polymer substrates can potentially be used for development of flexible electronics and lab-on-chip systems. In this study, we investigated the effects of deposition parameters on the crystal structure of AlN thin films on polymer substrates deposited by reactive direct-current magnetron sputtering. The results show that low sputtering pressure as well as optimized N₂/Ar flow ratio and sputtering power is beneficial for AlN (002) orientation and can produce a highly (002) oriented columnar structure on polymer substrates. High sputtering power and low N₂/Ar flow ratio increase the deposition rate. In addition, the thickness of Al underlayer also has a strong influence on the film crystallography. The optimal deposition parameters in our experiments are: deposition pressure 0.38 Pa, N₂/Ar flow ratio 2:3, sputtering power 414 W, and thickness of Al underlayer less than 100 nm.

© 2012 Elsevier B.V. All rights reserved.

1. Introduction

Flexible electronics on polymer substrates has recently become an important research topic as it provides a low-cost alternative for high-performance electronic devices and circuits. Significant advances have been made to fabricate flexible devices and systems such as displays [1,2], thin film solar cells [3,4], sensors [5,6], thin film transistors [7], and RF/microwave circuits [8]. Microelectromechanical system (MEMS) is an emerging class of electronic devices with unique electronic and mechanical functions and properties. They are usually fabricated on rigid substrates such as Si and glass. MEMS on flexible substrates could offer great advantages over those on rigid substrates as they are robust, light-weight, low-cost, and are able to absorb mechanical stress [9]. Various MEMS devices have been built on polymer substrates, such as micromachined infrared bolometers [10], piezoelectric actuators [11], and microfluidics [12].

Aluminum nitride (AlN) possesses some unique properties such as high piezoelectric constants, electromechanical coupling coefficient, degree of hardness, acoustic speed, and dielectric constant. It is one of most important materials for fabrication of piezoelectric sensors and actuators, surface acoustic wave devices, and film bulk acoustic resonators (FBARs). Various attempts have been made to develop

AlN-based MEMS on flexible polymer substrates [13–16]. For these applications, the key is to grow c-axis oriented AlN thin films on such substrates. Akiyama et al. [13] have deposited AlN on polyimide substrates and demonstrated piezoelectric effect upon pressure variation, though the piezoelectric coefficient is much lower than that of the bulk material. With the same structure, they also investigated a combination of high and low-modulus materials (AlN thin films and polyimide films, respectively) in diaphragms for high-sensitivity response [14]. Bu et al. [15] developed a method to measure muscle movement using a flexible piezoelectric thin film sensor made of an oriented AlN film. Petroni et al. [16] fabricated piezoelectric transducers consisting of a molybdenum (Mo) top electrode, an AlN active layer, and a Mo bottom electrode on a Dupont Kapton HN polymeric tape.

Many attempts have been made to deposit AlN on rigid substrates by varying the underlayer materials and deposition conditions such as pressure, substrate temperature, gas ratio etc. High-quality AlN films have been obtained with controllable preferred crystal orientation, mainly (002) [17]. However, growth of AlN on flexible substrates is very different from that on rigid substrates due to temperature limitations, differences in thermal expansion coefficient, and amorphous state of the polymer substrates, thus presenting a technological challenge to deposit high-quality AlN films on flexible substrates. Although some effort has been made to fabricate AlN thin film-based devices on polymer substrates, the research is at a very early stage. How the deposition conditions and underlayer affect the growth of

* Corresponding author. Tel./fax: +86 57187951710.

E-mail address: hjin@zju.edu.cn (H. Jin).

the crystal structure remains highly unclear at this time. And the properties of the thin films on flexible substrates and the deposition process are far from optimized. In this paper, we report results on deposition of AlN thin films on polyimide substrates by reactive direct-current (DC) magnetron sputtering without intentional heating, and elucidate the effects of deposition parameters and underlayer on the crystal structure of the AlN films.

2. Experiments

A Kapton® polyimide film 100H (Toray, Dupont, thickness 25 μm) was chosen as the substrate for the deposition of Al layers owing to its excellent mechanical and electrical properties, chemical stability, and wide operating temperature range ($-269\text{ }^{\circ}\text{C}$ to $+400\text{ }^{\circ}\text{C}$). AlN was deposited using a DC magnetron sputtering system built in our laboratory. The base pressure of the chamber was $1 \times 10^{-4}\text{ Pa}$ before deposition. The Al target with purity 99.999% and diameter of 60 mm was water-cooled. The distance between the target and the substrate was fixed at 70 mm. The size of polyimide used as substrate is 80 mm \times 80 mm, on which a grounded aluminum mask with a 60 mm-diameter opening is placed, resulting in an area of deposited AlN film with the same diameter. Before depositing the AlN film, an Al underlayer was deposited on the polyimide substrate as a transitional electrically conducting layer with deposition pressure of 0.27 Pa and DC power of 300 W as Al can be used as the bottom electrode for fabrication of FBARs. AlN was then deposited on the Al coated polyimide substrate in N_2/Ar atmosphere. The effect of deposition conditions such as pressure, N_2/Ar flow ratio, and DC sputtering power, as well as thickness of the Al underlayer, on the properties of the AlN films was investigated. Table 1 summarizes the deposition parameters for four groups of samples. All samples were deposited for 1 h without intentionally heating the substrates.

The crystalline structure and crystal orientation of films were analyzed using X-ray diffraction (XRD) (Shimadzu XRD-6000) with $\text{Cu-K}\alpha$ radiation ($\lambda = 0.154\text{ nm}$) working at 40 kV and 36 mA. The diffraction patterns were obtained in the 2θ model with scanned angle of $2\theta = 20^{\circ} - 70^{\circ}$. The degree of c-axis crystallization was examined at full-width at half maximum (FWHM) of the AlN (002) diffraction peak. The strain and crystallite size of the thin film were extracted from the XRD data using a standard methodology [18]. Strain is

calculated from $\varepsilon_z = (c - c_0)/c_0$, where c_0 is the strain-free lattice constant (4.979 Å) and c the lattice constant which is equal to twice the interplanar spacing d , measured from the position of the (002) peak using the Bragg equation. Crystallite grain sizes were calculated from the Debye–Scherrer formula: $D = K\lambda/(\beta \cos \theta)$, where K is the shape factor of the average crystallite with a value of 0.94, λ the X-ray wavelength (1.5405 Å for Cu target), β the FWHM in radians, θ the Bragg angle, and D the mean crystallite grain size normal to diffracting planes. The crystallinity is analyzed with MDI Jade 5.0 software, and is deduced from the ratio of diffraction peak intensity to total intensity. For cross-sectional structure analysis, a Scanning Electron Microscope (SEM) (Hitachi S-4800) was used at the accelerating voltage of 5 kV. The morphology of roughness of the film surfaces was observed by atomic force microscopy (AFM) (SPI-3800N, Seiko Co.) under tapping mode. Tap300Al-G Si probes (Budget sensors AFM probes, Sofia, Bulgaria) were used with the normal resonant frequency of 300 kHz.

3. Results and discussion

The effects of deposition pressure, N_2/Ar flow ratio, sputtering power, and Al underlayer thickness are discussed in the following subsections, respectively. By changing one deposition parameter while fixing the other three, we examine the effect of each on the properties of AlN thin film, leading to an optimized set of deposition parameters.

3.1. Deposition pressure

The deposition pressure was varied and values of 0.38, 0.45 and 0.53 Pa were used with a fixed N_2/Ar gas flow ratio of 1:1 (55:55 sccm) and sputtering power of 266 W (1 A, 266 V) to investigate the effect on the crystal structure of the AlN films. Fig. 1 shows the XRD pattern of the AlN films deposited under different deposition pressures. Each AlN film shows a main XRD peak near $2\theta = 36.1^{\circ}$ which corresponds to the AlN (002) crystal orientation. The results demonstrated that the AlN crystal structures are perpendicular to the polymer substrate with a (002) orientation. It is clear from the figure that with the increase of pressure, the intensity of the AlN (002) peak decreases. Further, as shown in Fig. 2, the FWHM of the AlN (002) peak increases as the grain size decreases, consistent with the results of the AlN films deposited on rigid substrates such as Si [19] and Sapphire [20]. The decreased intensity of the XRD indicates that increased amorphicity presents in the film. As increasing the deposition pressure leads to the decrease of kinetic energy of sputtered

Table 1
Deposition parameters for AlN thin films by reactive DC magnetron sputtering.

Sample no.	Deposition parameters ^a			
	Deposition pressure (Pa)	N_2/Ar flow ratio	Sputtering power (W)	Thickness of Al underlayer (nm)
A1	0.38			
A2	0.45	1:1	266	
A3	0.53			
B1		1:4		
B2		1:2		
B3	0.38	2:3	266	
B4		1:1		
B5		3:2		100
C1			100	
C2			183	
C3	0.38	2:3	266	
C4			351	
C5			414	
C6			504	
D1				18
D2				35
D3	0.38	2:3	414	70
D4				100
D5				200

^a Other deposition parameters are: Al target with purity 99.999%, 70 mm target-substrate distance, unheated substrate.

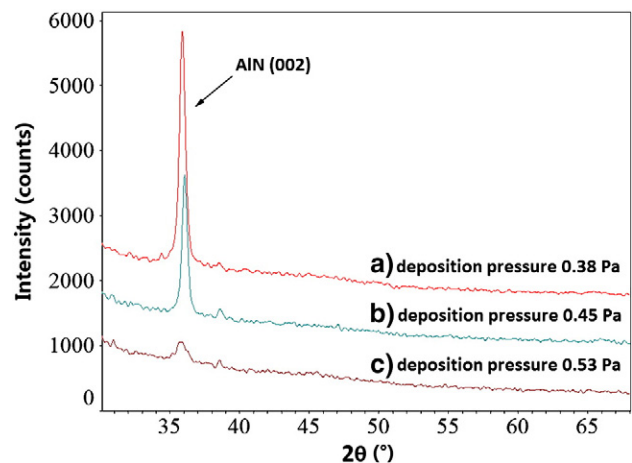


Fig. 1. XRD patterns of AlN thin films deposited on polymer substrates with Al electrodes under different deposition pressures (the different spectra are presented on top of each other for clarity).

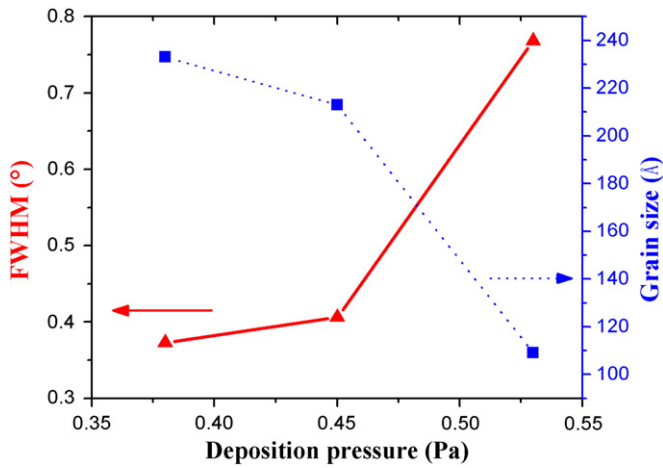


Fig. 2. The effect of deposition pressure on the FWHM of XRD of AlN (002) thin films.

atoms and to a low surface mobility of the condensing species, especially at low deposition temperatures [21], the (002) crystallization decreases as the pressure increases. The lowest deposition pressure is 0.38 Pa, beyond which the glow discharge disappears.

Fig. 3 shows SEM micrographs of the cross-sectional structure of the AlN films deposited on polymer substrate at different deposition pressures, and Fig. 4 shows the AFM images. Each AlN film exhibits a typical (002) oriented columnar structure. The surface of the film deposited at 0.38 Pa is smoother than the other two films, and the columns are more neatly arranged and compact. The mounds that appear in Fig. 3(a) may be dust particles, since the experiments were not performed in a clean room. As the pressure increased, the surface became rougher and the structure became much coarser and non-columnar, consistent with the XRD-result. This phenomenon can be explained by considering the scattering events and adatom mobility. At high deposition pressure, the probability of scattering increases and more particles lose their kinetic energy via collisions, resulting in lower adatom surface mobility. Generally, higher adatom mobility promotes the growth of the AlN thin film with a c-axis orientation, because if the particles have higher mobility they are more likely to find the low energy binding sites which leads to crystal growth. Furthermore, at high deposition pressure, the tendency for film bombardment by particles at an oblique angle increases due to scattering, resulting in low film density.

3.2. N_2/Ar flow ratio

The effect of the N_2/Ar gas flow ratio on the crystal structure of the AlN films on polymer substrates has been investigated at a fixed sputtering power of 266 W (1 A, 266 V) and deposition pressure of 0.38 Pa. Fig. 5 shows the dependence of the FWHM and deposition rates on the N_2/Ar gas flow ratio. The results show that the sample deposited with a N_2/Ar flow ratio of 2:3 has a minimum FWHM of 0.306° , implying an optimum gas flow ratio for the best crystal quality. The degree of AlN (002) texture improves as the N_2/Ar flow ratio was increased from 1:4 to 2:3, and decreases with further increase of the flow ratio. Hang et al. [22] pointed out that a high N_2/Ar flow ratio is beneficial for depositing AlN films with the desired c-axis orientation. The flux of the bombarding particles increases with the N_2/Ar flow ratio which enhances the mobility of adatoms on the film surface, thus beneficial for the growth of the (002) AlN oriented crystal. On the other hand, too much N_2 leads to superfluous N elements and Al vacancies in the films, resulting in a high density of defects and poor-quality AlN films. Therefore, there exists an optimal N_2/Ar flow ratio for well-defined c-axis orientation and crystal structure. Fig. 5 also shows the corresponding deposition rate which continuously decreases with the increase of gas flow ratio owing to the low sputtering yield of the Al target by N^+ bombardment and the target poisoning effect [23].

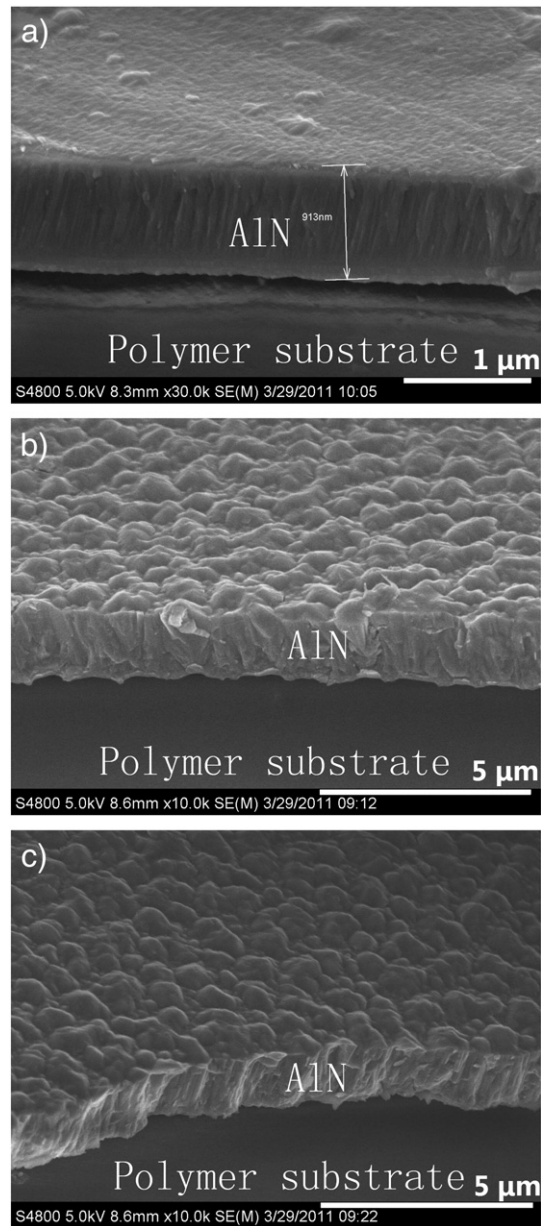


Fig. 3. The SEM images of AlN thin films on polymer substrates with Al electrodes under different deposition pressures: (a) 0.38 Pa; (b) 0.45 Pa and (c) 0.53 Pa.

The AlN thin films deposited at higher N_2/Ar flow ratios exhibited a higher crystallinity as shown in Figs. 6 and 7 owing to reduced nitrogen deficiency (nitrogen vacancies) [17]. As the N_2/Ar flow ratio increases, the grain size increases from 230 Å to 290 Å at a N_2/Ar flow ratio of 2:3, and then reduced to 228 Å at a N_2/Ar flow ratio of 3:2. The microstructure and morphology of the films is shown in Fig. 7. All films exhibit a typical (002) oriented columnar structure from the XRD curves. However, from the SEM images it is clear that the films deposited at low N_2/Ar flow ratio shows fine grains, and the columnar structure gradually becomes more pronounced with the increase of N_2/Ar flow ratio. Based on these results, we conclude that the optimal N_2/Ar flow ratio is around 2:3.

3.3. Sputtering power

Generally, high sputtering power is beneficial for growth of AlN with an (002) orientation, since the incident atoms have sufficiently high energies to allow growth normal to the substrate [17]. However,

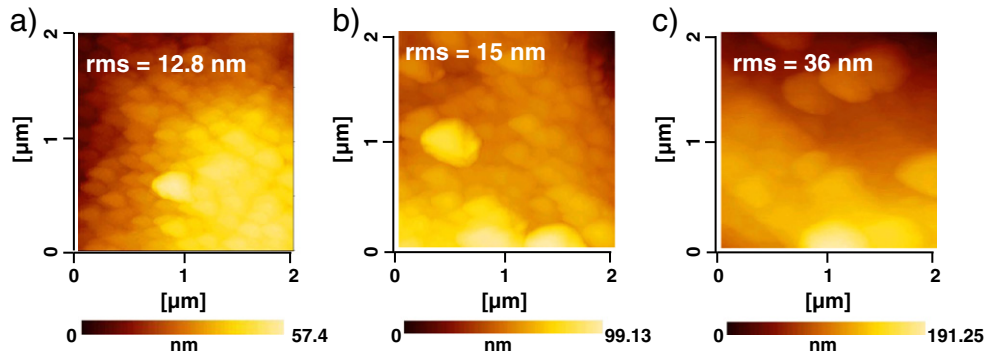


Fig. 4. The AFM images of AlN thin films on polymer substrates with Al electrodes under different deposition pressures: (a) 0.38 Pa, (b) 0.45 Pa, and (c) 0.53 Pa.

for deposition of thin films on polymer substrates, high sputtering power may damage the polymer substrates significantly, causing curling and burning. Therefore, the power must be optimized to obtain the best crystal structure yet retain the integrity of the substrate. Sputtering power was varied to elucidate its effect on the properties of the AlN film on polymer substrate. The power used was 100 W (0.4 A, 252 V), 183 W (0.7 A, 262 V), 266 W (1 A, 266 V), 351 W (1.3 A, 270 V), 414 W (1.5 A, 276 V) and 504 W (1.8 A, 280 V), with a fixed deposition pressure of 0.38 Pa and N_2/Ar flow ratio of 2:3. It was found that the AlN films crack and peel off from the polymer substrates once the sputtering power is larger than 504 W, and this is believed to be caused by the large difference in thermal expansion coefficients between the substrate and the film at high temperatures.

Fig. 8 shows the XRD patterns of these samples and Fig. 9 shows the FWHM and deposition rate of the corresponding samples. The intensity of the AlN (002) peak increases, while the FWHM decreases from 0.62° to 0.346° when the sputtering power reaches 414 W. The results demonstrated that the (002) crystal orientation is enhanced with increase in sputtering power, consistent with the results obtained by others on rigid substrates [17,24]. It is believed that a reasonably high sputtering power could increase not only the sputtering yield, but also the incident particle kinetic energy which enhances the mobility of the atoms deposited and the migration distance, thus beneficial for the growth of (002) oriented crystallites [24]. However, once the sputtering power exceeded 500 W, the intensity of the AlN (002) peak is reduced and the FWHM increases to 0.376° . This may be caused by the deterioration of the substrate at high temperatures at high power deposition as evidenced by the peeling off of the samples deposited at powers higher than 500 W, and/or insufficient atom migration at such a high deposition rate and the high energy incident

atoms. At high deposition rate, atoms do not have sufficient time to rearrange on the surface before the next atoms are deposited, leading to a deteriorated crystal structure. Furthermore, the incident atoms have very high energy, which can damage the surface of the newly formed AlN layer, thus destroying the (002) crystal orientation.

Fig. 10 shows the dependence of strain and grain size on the deposition power. The grain size increases from $\sim 130 \text{ \AA}$ to $\sim 250 \text{ \AA}$ with increase in deposition power up to 414 W. As the power increases further, the grain size reduces. This is probably due to the deposition of mixed crystal and amorphous phases at such high deposition rate, leading to reduced grain sizes. The strain was found to be $< 0.5\%$ for all deposition powers except 100 W, and decreased with increase in deposition power, contrasting most observations on rigid substrates. It is generally understood that the strain of thin films deposited by physical vapor depositions on rigid substrates normally increases with deposition power due to increased impinging energy at high powers [25]. For polymer substrate, high-power deposition may increase the substrate temperature, thus “softening” the substrate, leading to stress relaxation, as evidenced by peel-off of the films at a power over 500 W.

Fig. 11 shows the SEM micrographs of AlN films on polymer substrates at different sputtering powers. It is clear that thickness increases with increase in power, and as shown in Fig. 11(b) and (c), there exists a thin transition region between the (002) oriented AlN film and the polymer substrate where the film is randomly oriented relative to the columnar structure, which is consistent with the observation for (002) AlN films deposited on rigid Si substrates [26]. The lines in Fig. 11(c) were caused by scratches on the polyimide substrate, since the polyimide substrate is very thin and not completely planar. These results imply that the early film growth is a random

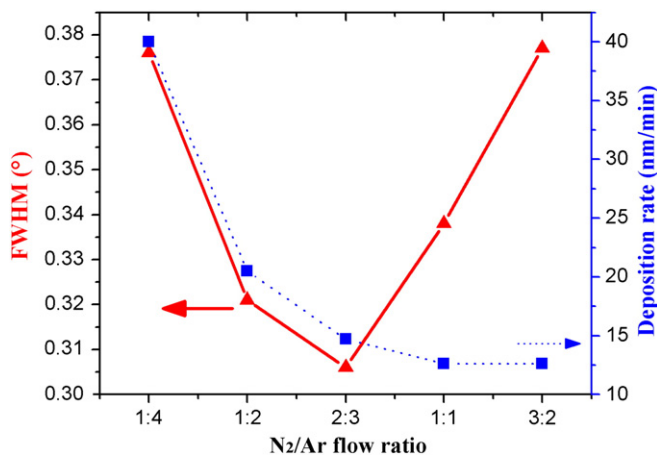


Fig. 5. The effect of N_2/Ar flow ratio on the FWHM of XRD curves and the deposition rate of AlN thin films.

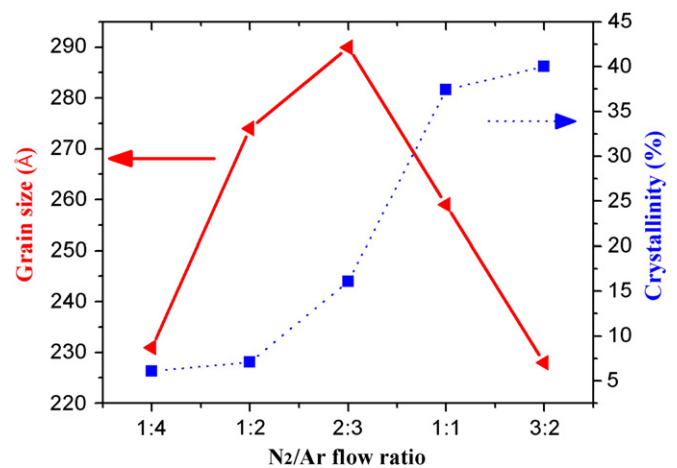


Fig. 6. The effect of N_2/Ar flow ratio on the grain size and crystallinity of AlN (002) thin films.

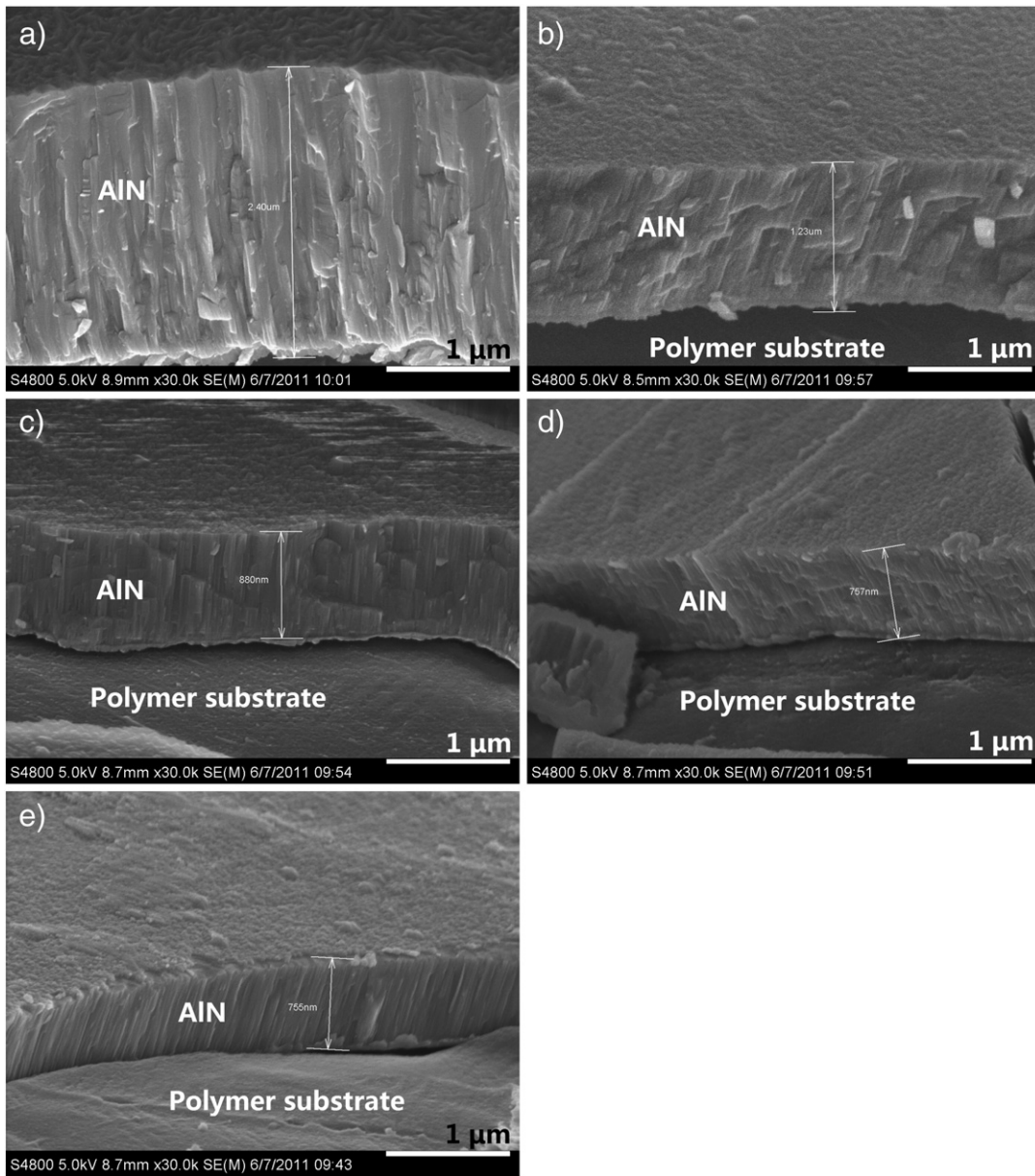


Fig. 7. The SEM images of AlN thin films on polymer substrates under N_2/Ar flow ratios of (a) 1:4; (b) 1:2; (c) 2:3; (d) 1:1 and (e) 3:2.

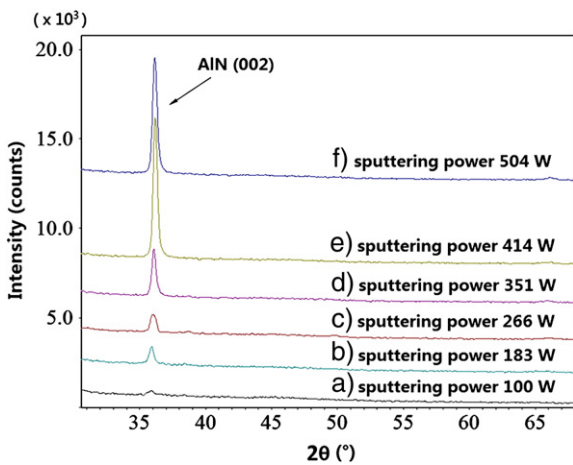


Fig. 8. XRD patterns of AlN thin films deposited on polymer substrates under different sputtering powers (the different spectra are presented on top of each other for clarity).

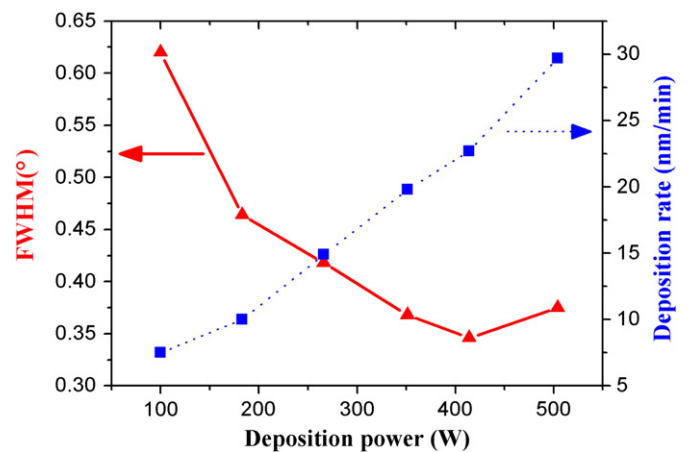


Fig. 9. The effect of sputtering power on the FWHM of XRD and the deposition rate of AlN thin films.

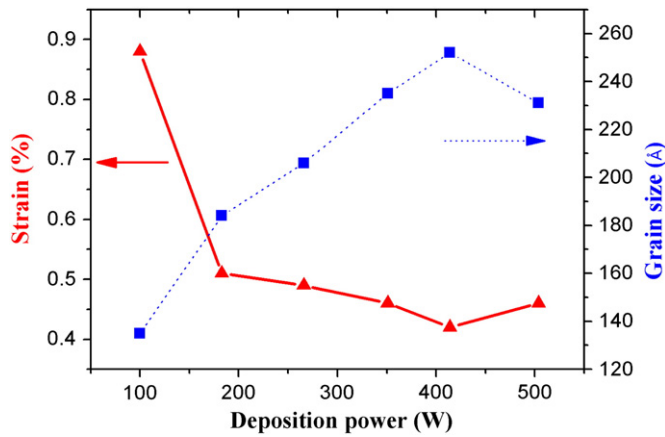


Fig. 10. The effect of sputtering power on the strain and grain size of AlN thin films.

and non-oriented process and the preferred (002) crystal orientation becomes dominant after transitional growth [21].

3.4. Underlayer thickness

Al is used as the underlayer for growth of AlN in this study. It serves as a transition layer to improve the quality of the AlN thin film as well as an electrode for the development of FBAR devices, the ultimate objective of the project. Fig. 12 shows XRD patterns for the AlN thin films deposited on an Al underlayer with thicknesses of 18, 35, 70, 100 and 200 nm, respectively. Fig. 13 shows the dependence of grain size and strain that were extracted from the XRD-curves on the Al layer [18]. The deposition conditions were fixed at a pressure of 0.38 Pa, a N_2/Ar flow ratio of 2:3 and a power of 414 W (1.5 A, 276 V). The thickness of the Al layer was controlled by varying the deposition time at a fixed DC power of 300 W.

It is obvious that with the increase in the Al underlayer thickness, the intensity of the (002) peak decreases, while that of Al (111)

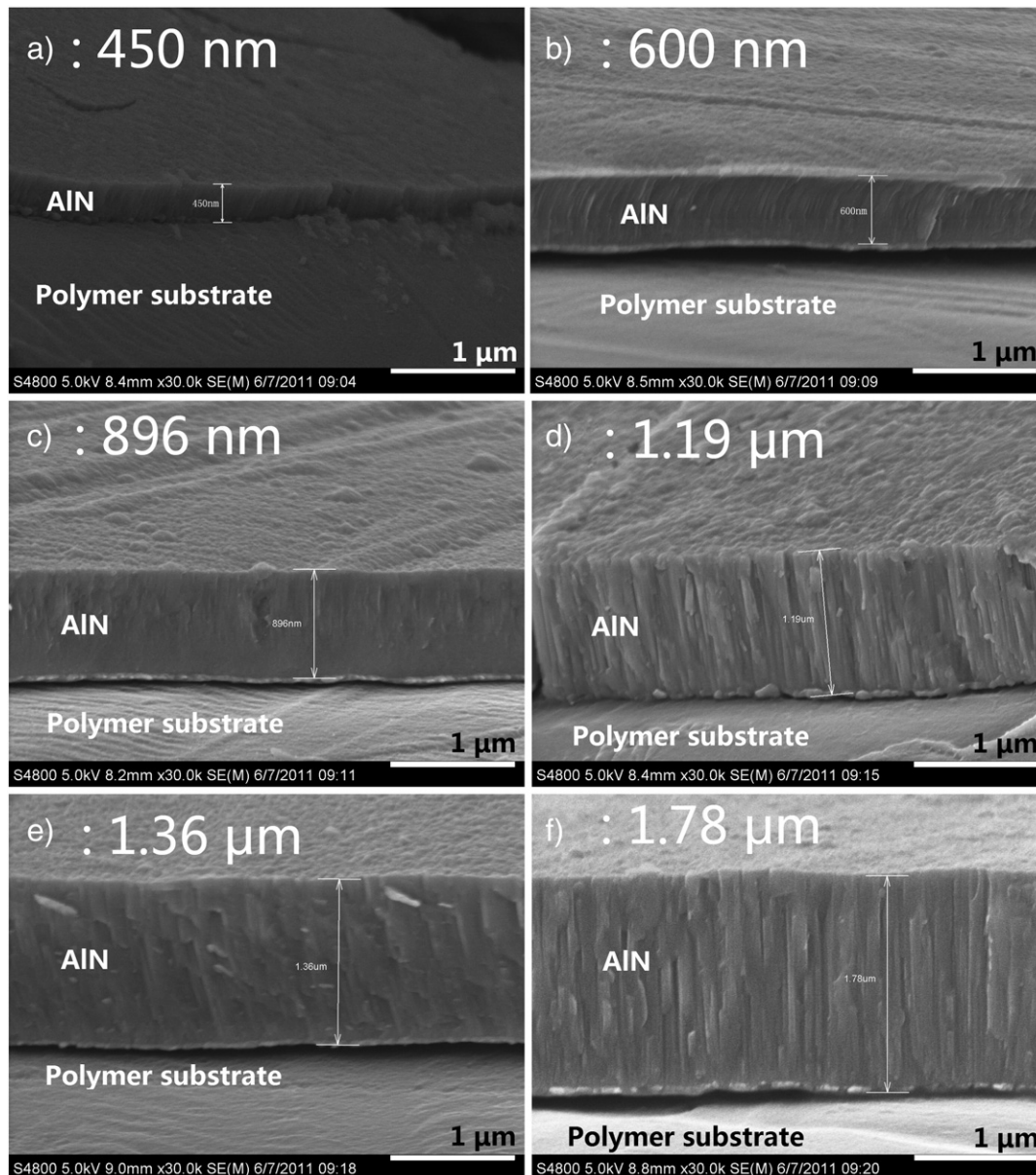


Fig. 11. The SEM images of AlN thin films on polymer substrates with Al electrodes under different sputtering powers of (a) 100 W; (b) 183 W; (c) 266 W; (d) 351 W; (e) 414 W and (f) 504 W.

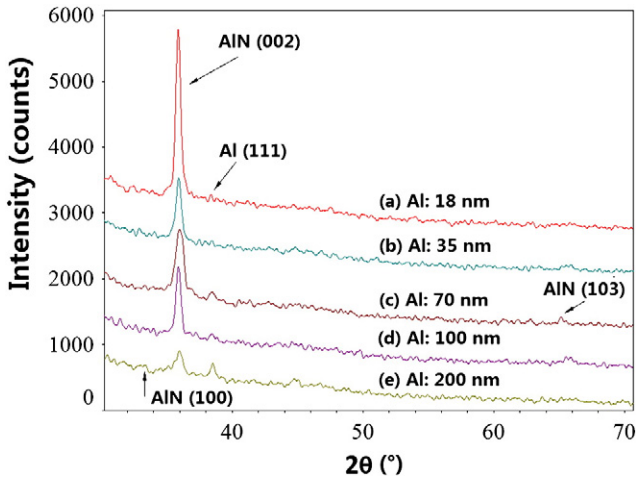


Fig. 12. XRD patterns of AlN thin films deposited on polymer substrates with different thicknesses of Al underlay (the different spectra are presented on top of each other for clarity).

increases. The sample with an 18 nm Al layer has the best quality, with a FWHM of AlN (002) being 0.416° and the grain size being 316 Å. As the Al underlayer thickness increases to 200 nm, the

FWHM of AlN (002) increases to 0.63° and the grain size decreases to 175 Å. Fig. 12 also shows that a thicker Al underlayer (70 nm, 100 nm, and 200 nm) leads to the formation of a mixture of AlN (002) and AlN (103) crystallites. The corresponding AlN (103) relative peak intensities are 8.5%, 8.6%, and 8.1%, respectively, compared to those of the AlN (002) peak. When the thickness of the Al underlayer is 200 nm, the peaks of many other crystals appear, indicating the formation of fine grain and randomly orientated crystals. AlN (100) orientation is observed and the relative peak intensity is 30% of that of AlN (002). A possible explanation is that thicker Al underlayers have larger surface roughness, leading to various crystal orientations. As shown in Fig. 13, the surface roughness of Al underlayer clearly increases with increase in thickness. The growth of AlN deposited on rough surfaces follows the crystals of Al with different orientations, leading to the formation of various AlN crystal orientations. The rough surface may also increase the migration distance for the adatoms, enhancing localized, non-preferential crystal growth. It is generally believed that underlayers with a preferred crystal orientation are needed for the growth of high-quality AlN layers as this can minimize the undesirable crystal orientation caused by lattice mismatch. However, some experiments have also shown highly c-axis oriented AlN thin films can be grown on different substrates as long as the rms roughness of the substrate surface is less than 4 nm, independent of the lattice mismatch between substrate and AlN [17]. Our results show that surface roughness is more important than the crystal orientation of the underlayer for (002) AlN growth. And the amorphous transition layer plays a key role in reducing the dependence of AlN film properties on substrate crystal orientation.

Fig. 14 shows the strain increases while the grain size decreases with increase in the Al underlayer thickness. The strain is about <0.5% for most of the samples and then abruptly increases to 0.63% when deposited on a 200 nm Al layer. The results show that the thickness of Al layer below 100 nm would be better for (002) oriented AlN growth. Fig. 15 shows the SEM images of these AlN samples. The microstructures of the deposited films are not homogeneous and have fine grain structures. Furthermore, the samples with the thinner Al underlayer have better columnar structures compared to those with thicker Al underlayer due to the decrease in surface roughness with decrease in underlayer thickness.

4. Conclusions

In this study, we investigated the synthesis and characteristics of AlN thin films on Dupont Kapton® polyimide film 100H polymer substrates with reactive DC magnetron sputtering. XRD and SEM were used to characterize the orientation, cross-sectional structure, surface morphology, and thickness of AlN thin films. Results show that at low deposition pressure, optimized N₂/Ar flow ratio, sputtering power and Al underlayer thickness are likely to yield AlN (002) orientation.

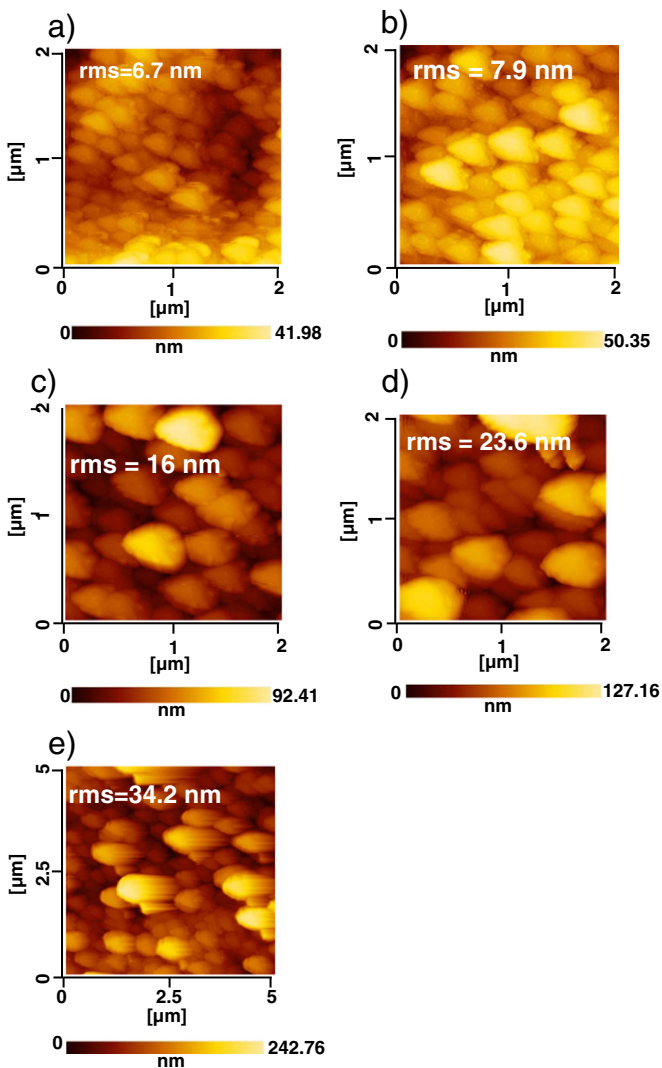


Fig. 13. The AFM images of Al underlayer with different thicknesses: (a) 18 nm, (b) 35 nm, (c) 70 nm, (d) 100 nm, and (e) 200 nm.

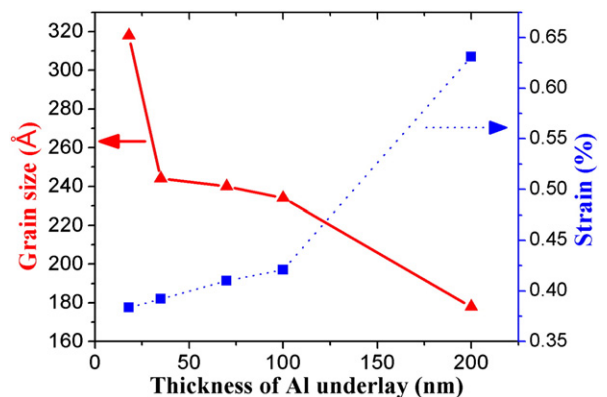


Fig. 14. The effect of Al underlayer on the strain and grain size of AlN thin films.

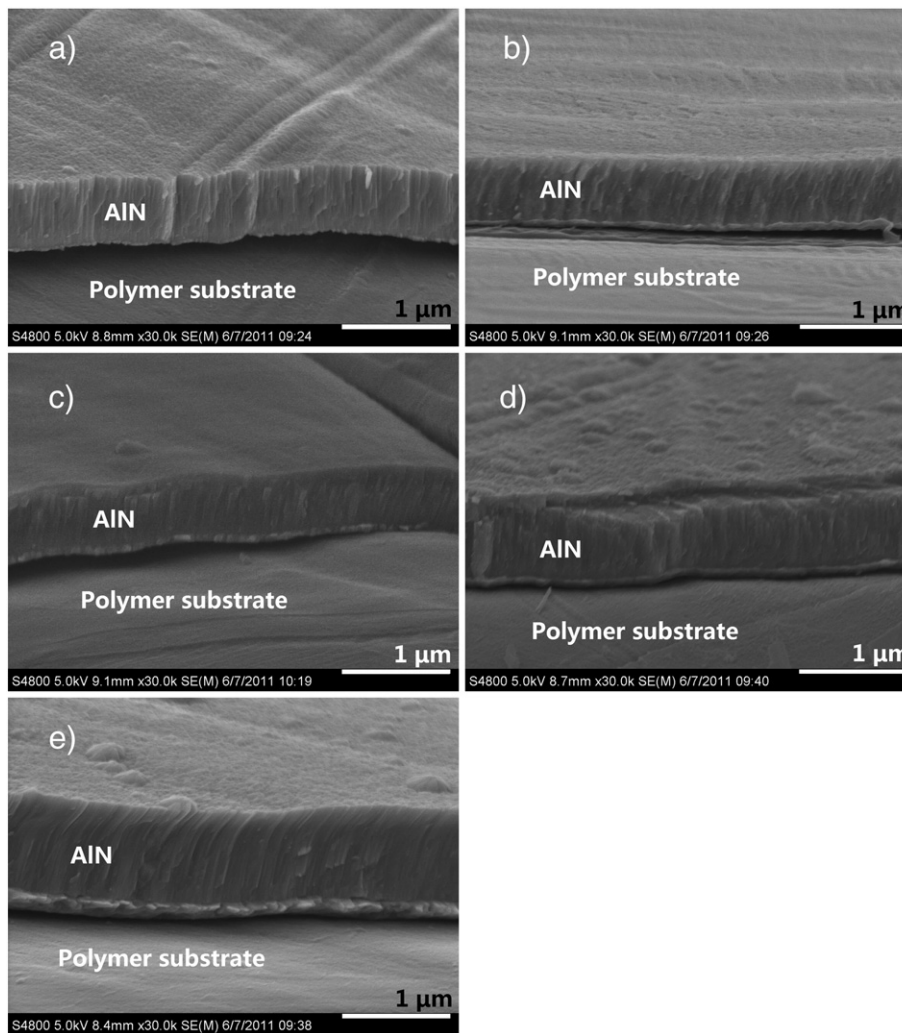


Fig. 15. The SEM images of AlN thin films deposited on polymer substrates with different thicknesses of Al underlayer: (a) 18 nm; (b) 35 nm; (c) 70 nm; (d) 100 nm and (e) 200 nm.

In addition, deposition rate is almost proportional to sputtering power and decreases with increase in N_2/Ar flow ratio. The Al underlayer has strong influences on the AlN film crystallography. In these experiments, the optimal deposition parameters for depositing (002) oriented AlN films on polymer substrates are at a deposition pressure of 0.38 Pa, N_2/Ar flow ratio of 2:3, and sputtering power of 414 W (1.5 A, 276 V), with an underlayer Al thickness below 100 nm.

Acknowledgments

This work was supported by the National Natural Science Foundation Key Program of China (No. 60936002), the National Natural Science Foundation China (No. 61171038), the Engineering and Physical Sciences Research Council (EP/F06294X/1) and the Royal Society International Joint Project with China (JP090873).

References

- [1] T. Hanada, T. Negishi, I. Shiroishi, T. Shiro, *Thin Solid Films* 518 (2010) 3089.
- [2] K.A. Sierros, D.R. Cairns, J.S. Abell, S.N. Kukureka, *Thin Solid Films* 518 (2010) 2623.
- [3] J.S. Cho, S. Baek, J.C. Lee, *Sol. Energy Mater. Sol. Cells* 95 (2011) 1852.
- [4] Y.-Y. Yu, W.-C. Chien, C.-Y. Ciou, H.-C. Wu, *Thin Solid Films* 519 (2011) 4721.
- [5] E. Zampetti, L. Maiolo, A. Pecora, F. Maita, S. Pantalei, A. Minotti, A. Valletta, M. Cuscunà, A. Macagnano, G. Fortunato, A. Bearzotti, *Sens. Actuators B* 155 (2011) 768.
- [6] F.-Y. Chang, R.-H. Wang, H. Yang, Y.-H. Lin, T.-M. Chen, S.-J. Huang, *Thin Solid Films* 518 (2010) 7343.
- [7] K.-H. Cho, M.-G. Kang, S.-M. Oh, C.-Y. Kang, Y. Lee, S.-J. Yoon, *Thin Solid Films* 518 (2010) 6277.
- [8] L. Sun, G. Qin, H. Huang, H. Zhou, N. Behdad, W. Zhou, Z. Ma, *Appl. Phys. Lett.* 96 (2010) 013509.
- [9] D. Zhao, D.A. Mourey, T.N. Jackson, *IEEE Electron Device Lett.* 31 (2010) 323.
- [10] S.Y. Xiao, L.F. Che, X.X. Li, Y.L. Wang, *Microelectron. Eng.* 85 (2008) 452.
- [11] T. Lemke, G. Biancuzzi, H. Feth, J. Huber, F. Goldschmidtboing, P. Woias, *Sens. Actuators A* 168 (2011) 213.
- [12] E.J. Geiger, A.P. Pisano, F. Svec, *J. Microelectromech. Syst.* 19 (2010) 944.
- [13] M. Akiyama, Y. Morofuji, T. Kamohara, K. Nishikubo, Y. Ooishi, M. Tsubai, O. Fukuda, N. Ueno, *Adv. Funct. Mater.* 17 (2007) 458.
- [14] M. Akiyama, Y. Morofuji, K. Nishikubo, T. Kamohara, *Appl. Phys. Lett.* 92 (2008) 043509.
- [15] N. Bu, O. Fukuda, N. Ueno, M. Inoue, *IEEE International Conference on Robotics and Biomimetics*, IEEE, New York, 2009, p. 944.
- [16] S. Petroni, C.L. Tegola, G. Caretto, A. Campa, A. Passaseo, M.D. Vittorio, R. Cingolani, *Microelectron. Eng.* 88 (2011) 2372.
- [17] G.F. Iriarte, J.G. Rodriguez, F. Calle, *Mater. Res. Bull.* 45 (2010) 1039.
- [18] W.T. Lim, B.K. Son, D.H. Kang, C.H. Lee, *Thin Solid Films* 382 (2001) 56.
- [19] A. Ababneh, U. Schmid, J. Hernando, J.L. Sánchez-Rojas, H. Seidel, *Mater. Sci. Eng. B Adv.* 172 (2010) 253.
- [20] H. Seo, I. Petrov, K. Kim, *J. Electron. Mater.* 39 (2010) 1146.
- [21] J. Bjurström, D. Rosen, I. Katardjiev, V.M. Yanchev, I. Petrov, *IEEE Trans. Ultrason. Ferroelectr. Freq. Control* 51 (2004) 1347.
- [22] C.L. Huang, K.W. Tay, L. Wu, *Solid State Electron.* 49 (2005) 219.
- [23] S. Berg, T. Nyberg, *Thin Solid Films* 476 (2005) 215.
- [24] K.H. Chiu, J.H. Chen, H.R. Chen, R.S. Huang, *Thin Solid Films* 515 (2007) 4819.
- [25] M. Ohring, *Materials Science of Thin Films*, Second edition, Academic Press, 2001.
- [26] H. Cheng, Y. Sun, P. Hing, *Thin Solid Films* 434 (2003) 112.